Title

Kinetic study of shock formation and particle acceleration in laser-driven quasi-parallel magnetized collisionless shocks

Journal

Physics of Plasmas, 31(8)

ISSN

1070-664X

Authors

Zhang, Yu
Heuer, Peter V
Davies, Jonathan R
et al.

Publication Date

2024-08-01

DOI

10.1063/5.0210050

Kinetic study of shock formation and particle acceleration in laser-driven quasi-parallel magnetized collisionless shocks

Yu Zhang,[1,2] Peter V. Heuer,[1] Jonathan R. Davies,[1,2] Derek B. Schaeffer,[3] Han Wen,[1] Fernando García-Rubio,[1] and Chuang Ren[1,2,4]

[1)]*Laboratory for Laser Energetics, University of Rochester, Rochester, New York 14623, USA*

[2)]*Department of Mechanical Engineering, University of Rochester, Rochester, New York 14627, USA*

[3)]*Department of Physics and Astronomy, University of California-Los Angeles, Los Angeles, California 90095, USA*

[4)]*Department of Physics and Astronomy, University of Rochester, Rochester, New York 14627, USA*

(*Electronic mail: chuang.ren@rochester.edu)

(Dated: 3 July 2024)

Quasi-parallel magnetized collisionless shocks are believed to be one of the most efficient accelerators in the universe. Compared to quasi-perpendicular shocks, quasi-parallel shocks are more difficult to form in the laboratory and to simulate because of their large spatial scales and long formation times. Our two-dimensional particle-in-cell simulations show that the early stages of quasi-parallel shock formation are achievable in experiments planned for the National Ignition Facility and that particles accelerated by diffusive shock acceleration (DSA) are expected to be observable in the experiment. Repetitive ion acceleration by crossings of the shock front, a key feature of DSA, is seen in the simulations. Other characteristic features of quasi-parallel shocks such as upstream wave excitation by energetic ions are also observed, and energy partition between ions and electrons in the downstream of the shock is briefly discussed.

I. INTRODUCTION

Magnetized collisionless shocks are ubiquitous in the universe and are presumed to be the source of some of the highest energy cosmic rays. Fermi acceleration was first proposed to account for the origin of the inverse power law spectral distribution of these cosmic rays[1]. In Fermi's theory, interstellar particles interact with wandering magnetic fields and gain energy from experiencing more head-on collisions than overtaking collisions. The stochastic mechanism is often known as "magnetic mirrors", or second-order Fermi acceleration. Fermi's theory was further developed and referred to as diffusive shock acceleration (DSA) in the late 1970s[2–5], which is associated with particle acceleration in strong shock waves, such as supernova explosions[6]. DSA requires particles to have large enough gyro-radii to pass through the shock without strong deflection in order to be accelerated. However, how particles acquire the initial energy required to do this remains an open question (the "injection" problem). It is generally believed that ions can fulfill the condition for DSA more easily than electrons because of their larger Larmor radii compared to the shock thickness[7]. Although DSA theory has been used to account for observations, direct evidence remains scarce.

In magnetized shocks, the angle θ_n between the shock normal and external magnetic field is a fundamental feature that dictates key shock characteristics. The angle θ_n is used to categorize magnetized shocks into quasi-perpendicular ($\theta_n > 45^\circ$) and quasi-parallel ($\theta_n < 45^\circ$) geometries. Unlike quasi-perpendicular shocks, which can be formed on timescales less than an ion gyro-period[8–11], quasi-parallel shocks rely on ion-ion instabilities that grow slowly and therefore are much more difficult to form. Consequently, while quasi-perpendicular shocks have been successfully created on several laser facilities[12–15], quasi-parallel shocks have yet to be created experimentally, due to the high laser energy required to enable a sufficiently large plasma, among other constraints[10]. Quasi-parallel shocks are believed to be more efficient accelerators of particles than quasi-perpendicular shocks[16].

As a complement to astronomical observations, laboratory shock experiments driven by lasers can provide a repeatable, and systematic way of studying collisionless shock physics[17], and advanced diagnostic systems provide additional measurements and characterizations that are not possible in space. Laboratory experiments can access early stages of shock formation, while astrophysical shocks are typically already fully formed. The laboratory formation of quasi-parallel collisionless shocks requires the combination of large magnetized system size and strongly-driven flows so that the shocks have sufficient space and time to develop and accelerate particles while still remaining collisionless. For example, the density of the laser-produced plasma must be low enough that Coulomb collisions remain negligible, but high enough to fit hundreds of ion inertial lengths that allow the shock formation in the experimental apparatus; the applied magnetic field must be strong enough to magnetize the plasma, but weak enough to satisfy the Mach number requirement[10]. The experimental and physical constraints rule out most of the existing laser facilities. Our experiments are currently underway to achieve these conditions by utilizing the National Ignition Facility (NIF), the world's largest laser facility[18–22].

Earlier NIF experiments have observed unmagnetized collisionless shocks and associated energized electrons[23], and previous quasi-perpendicular shocks have observed proton energization[15]. Some of the beam instabilities that contribute to parallel shock formation have been observed at

the LAPD[24,25]. However, there is as yet no direct evidence of shock-accelerated particles from quasi-parallel laser-driven experiments available, which are more relevant to astrophysical observations. Numerical simulations can play a key role in facilitating the design of laboratory experiments on quasi-parallel shocks. Previous hybrid simulations[16,26,27] revealed much information on shock formation and particle acceleration, including acceleration efficiency, magnetic field amplification, and particle diffusion. However, hybrid studies utilize the kinetic-proton and fluid-electron model intrinsically and assume a Maxwellian thermodynamically equilibrium for electrons. Recent works[28–30] consider energy exchange between the ions and electrons in collisional plasma. In contrast, full particle-in-cell (PIC) simulations, which treat both ions and electrons kinetically, allow a self-consistent collsionless kinetic ion-electron energy exchange, which will be shown to be important under experiment-relevant conditions [see Section IV(B)].

In this paper, PIC simulations are used to study the formation of quasi-parallel collisionless shock and particle acceleration, relevant to NIF experimental parameters. With PIC simulations, not only are shock formation and ion acceleration studied, but also electron spectra are obtainable. Upstream waves generated by reflected high-energy particles are identified as Alfvén waves and magnetosonic waves. The downstream ion-electron energy partition is found to be on the order of unity, which is far from independent heating, implying a significant ion-electron energy exchange in the downstream.

This paper is organized as follows: Section II presents the simulation setup. The formation of quasi-parallel shocks within the parameter range achievable on the NIF at different oblique angles θ_n, shock structures, and ion acceleration are discussed in Section III. This section also gives a comparison of the acceleration capabilities of quasi-parallel and quasi-perpendicular shocks. Section IV briefly discusses upstream wave excitation, and ion-electron energy exchange observed in the downstream. Conclusions are given in Section V.

II. SIMULATION SETUP

The simulations are designed to model experiments currently underway on the NIF. In those experiments, a laser-driven piston plasma expands supersonically into an ambient magnetized plasma. The piston acts to sweep out magnetic flux and ambient particles, accelerating them to super-magnetosonic speeds and driving a collisionless shock[13,14,31]. To achieve quasi-parallel shocks, the piston is designed to expand at an angle of $\theta_n = 30^\circ$ relative to an externally applied background magnetic field. The size of the ambient plasma extends for several hundred ion inertial lengths, allowing the shock to propagate for several tens of ion gyro-times. The schematic of the experimental setup is shown in Fig. 1(a). Additional details on the experimental setup will be reported in a future paper.

The simulations are performed using OSIRIS 4[32], a fully kinetic, relativistic, parallel PIC code. Our simulations, shown schematically in Fig. 1(b), utilize a reflective wall (ideal

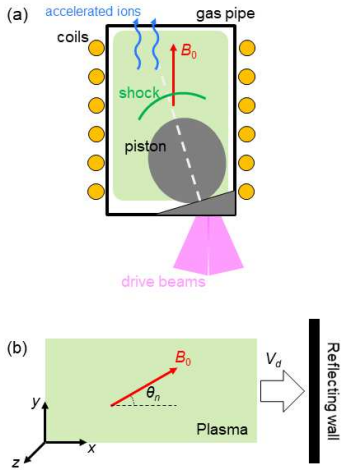

FIG. 1. (a) Experimental schematic on the NIF. (b) Wall-piston rest frame PIC simulation setup.

piston) boundary condition. Instead of simulating a piston plasma, a fixed reflective wall is implemented on the right boundary, from which a clear downstream, free of the influence of the piston, is obtained. This setup simplifies piston-ambient coupling[11,13,14,31] via ambient-wall collision and focuses on the shock itself. Magnetized plasma drifting against the wall ($+x$) with a bulk velocity of V_d is reflected off the wall and forms a shock that propagates to the left ($-x$) in the simulation. This ideal wall is a good analog for the solid-density piston in the experiments[8]. The simulations run in a piston/wall frame of reference, in which most of the figures in this paper are shown, except where the laboratory frame is explicitly stated in the captions. The velocity transformation between the laboratory and simulation frame simply follows $\mathbf{v}^{\text{lab.}} = \mathbf{v}^{\text{sim.}} - V_d\mathbf{e_x}$, where the superscripts denote the frames of reference, $\mathbf{e_x}$ represents the unit vector in the x-direction.

Unlike perpendicular shock formation, where the ion-electron mass ratio is critical[8], the formation and evolution of quasi-parallel shocks are dominated by ion-scale physics[10,16,33,34]. A reduced ion mass of $m_i/m_e = 50$ is thus used in most of our two-dimensional (2-D) PIC simulations. Some key initial upstream parameters are summarized in Table I. To better describe the shock, the subscripts 1 and 2 are hereinafter used to denote the upstream and downstream, respectively. Our simulations use a rectangular simulation domain in the x-y plane, with a minimum size of 883 c/ω_{pi1} in the x-direction and 21 c/ω_{pi1} in the y-direction. The shock propagates in the negative x-direction, and the external B field is uniform in the x-y plane, at shock angle θ_n to the shock normal. In the y-direction, a periodic boundary condition is applied for particles and fields. The grid size is 0.5 c/ω_{pe1} and the time step is 0.35 ω_{pe1}^{-1} to ensure convergence. We

TABLE I. Experiment and PIC simulation parameters

		Experiments	Simulations
Density	n_{e1}	5×10^{19} cm^{-3}	
Temperature	$T_{e1}=T_{i1}=T_1$	100 eV	
Magnetic field	B_1	30 T	
Drift (piston) Alfvénic Mach No.	$M_{A1}=V_d/v_{A1}$	11	
Plasma beta	$\beta_1=8\pi k_B(n_{e1}T_{e1}+n_{i1}T_{i1})/B^2$	4.47	
Shock angle	θ_n	30°	0°, 15°, 30°, 60°
Ion-electron mass ratio	m_i/m_e	1836	50
Ion collisional mean free path	λ_{ii}	2.5 cm	4600 $c\omega_{pi1}^{-1}$

used 12 × 12 macro-particles per cell in the simulations to maintain a low numerical collision effect. The total energy is conserved within 0.1% in the simulations. The expected mean free path[35] between the piston ions and ambient ions $\lambda_{ii}\approx 2.5$ cm is comparable to the system size in the experiments, therefore the physics involved is fundamentally collisionless. In the simulations, the collision module in OSIRIS is turned off.

III. SHOCK FORMATION AND PARTICLE ENERGIZATION

A. Formation of quasi-parallel shocks

Quasi-perpendicular shocks in strongly magnetized cases relevant to kiloJoule, TeraWatt laser experiments like OMEGA EP[36–38], have been found to be mediated by a modified two-stream instability (MTSI) between incoming and reflected ions, so can be formed within an ion gyro-period[8]. The MTSI relies on magnetically tied electrons and unmagnetized (or weakly magnetized) ions, similar to the lower hybrid mode, and has a growth rate much larger than the ion gyro-frequency[8,39,40], thus resulting in a shock formation time much less than an ion gyro-period $T_{ci}(=2\pi/\omega_{ci})$. In the quasi-parallel regime, however, the absence of an effective MTSI causes a much longer shock formation time, on the order of ion gyro-periods.

The dependence of shock formation on the shock angle θ_n in a quasi-parallel geometry has been studied by 2-D PIC simulations for $\theta_n=0^\circ$, 15°, and 30°. Although shocks with smaller θ_n take longer to form, we found that supercritical shocks where reflected ions are present and important[34,41] can all be formed within a few ion gyro-periods, consistent with previous studies[42]. The 2-D density maps of three simulations are presented in Fig. 2, with y-averaged density profiles (solid lines) plotted as well. The three rows of Fig. 2 correspond to $t=3.15$, 6.30, 12.59 ω_{ci1}^{-1}, respectively. An effective density jump[43] $r(\equiv n_2/n_1)\gtrsim 4$, which indicates the formation of the shocks, is observed in Figs. 2(c), (e), and (g) at $\theta_n=0^\circ$, 15°, and 30°, respectively, despite different shock profiles. The 3-D adiabatic limit for the density jump is 4[43,44]. The observed higher density jump is an overshoot in this transition region. It relaxes toward 4 in the downstream region. The density compression builds up faster at $\theta_n=30^\circ$, within one ion gyro-period, while at smaller θ_n a similar compression takes longer to form. The shock foot, which consists of ions reflected from the shock front, is larger for smaller oblique angles because the ion trajectories are impeded by the perpendicular component of the magnetic field, namely, B_y. Those reflected ions then gyrate in the upstream along the B field lines, excite waves, and deposit their energy to the ambient plasma, which is called the "diffusion" process. Ultimately the upstream region reaches a finite length[16,26], and set an energy threshold, above which ions can escape from the shock. Therefore, as can be clearly distinguished in Figs. 2(c), (f), (i), the wave pattern in the foot shows a close correlation with the B field direction.

Therefore, based on the above simulation results, we will use $\theta_n=30^\circ$ as our main setup following the experiments. In this case, the quasi-parallel shock formation time can be as short as $\sim 3\omega_{ci1}^{-1}$ (∼1 ns in the experiments). This setup gives faster shock evolution than $\theta_n=0^\circ$, while preserving features of particle acceleration similar to $\theta_n=0^\circ$. Most importantly, as will be shown in the following section, the energy spectra of energized ions remain similar between the $\theta_n=30^\circ$ case and smaller angles within the time accessible in the experiments.

B. Ion crossing of the shock front and energization

In the theoretical picture of DSA, particles gain energy by interacting with the shock front. However, a one-time interaction can only increase the energy of a particle by a moderate amount. Particles interacting many times with the shock can achieve very high energies[45]. Repetitive acceleration by crossing the shock front, one of the key features of DSA theories, is seen in our simulations. However, the experimentally accessible time is far from the time required for DSA to fully develop a population of highly energized ions, which is on the order of hundreds or thousands of ion gyro-times. Therefore, even on the NIF, only the early stages of quasi-parallel shock formation and the DSA process are achievable. We therefore limit the total time in our PIC simulations to 40 ω_{ci1}^{-1} to determine experimentally relevant characteristics of accelerated particles. A longer simulation with a sustained shock potentially could yield similar power-law energetic particle distributions seen by the hybrid simulations[16,26,27].

The trajectories of some representative ions, in the $\theta_n=30^\circ$ simulation, are plotted in Figs. 3(a) t-x and (b) x-y plots, in which their kinetic energies are indicated by color. Note that

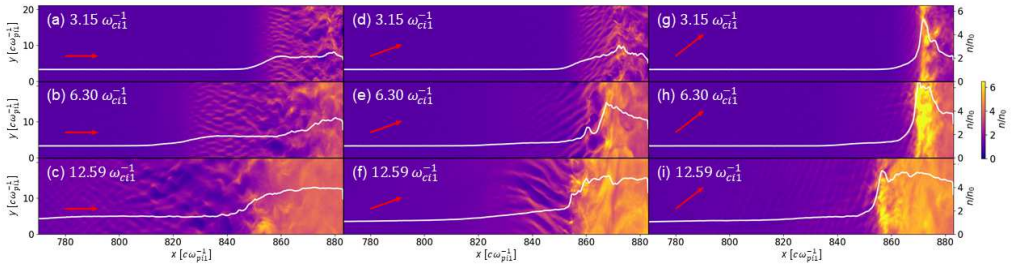

FIG. 2. 2-D ion density maps of quasi-parallel shocks with $\theta_n = $ (a-c) 0°, (d-f) 15°, and (g-i) 30°. The three rows top-to-bottom correspond to $t = 3.15, 6.30, 12.59\omega_{ci1}^{-1}$, respectively. The white solid lines are the y-averaged density profiles. The initial B field direction is marked with red arrows.

although the trajectories are given in the simulation frame for consistency, the particle energies are calculated in the laboratory frame throughout this paper. In Fig. 3(a), the y-averaged density profile is shown in the background in grayscale, and the shock front is plotted by the white dashed line. Tracked ions are repetitively reflected by the shock and gain energy by the Fermi process[1,3]. The maximum kinetic energy the ions can achieve within 40 ω_{ci1}^{-1}, comparable to the experiments, is ∼350 keV, which is ∼35× the shock energy (defined as $E_{sh} = \frac{1}{2} m_i V_{sh}^2 = 9.6$ keV, in which $V_{sh} = \frac{4}{3} V_d$ is used to approximate the shock velocity for a strong shock[43]). Figure 3(b) shows the 2-D trajectories in the x-y plane where the periodic boundary conditions in the y-direction are post-processed to show a continuous 2-D space. Accelerated ions gyrate along the B field lines in the upstream, which would make them convenient to collect experimentally [refer to Fig. 1(a)].

Figure 4 shows the history of particle energization, in which the energy spectra at different timesteps are plotted in different colors. Figures 4(a), (b), and (c) are the ion spectra for $\theta_n = 0°$, 30°, and 60°, respectively; the electron spectra are shown in Figs. 4(d), (e), and (f). Nonthermal particle populations are created by both the quasi-parallel and quasi-perpendicular shocks. However, spectra that extend further indicate that even at this early stage in their formation, quasi-parallel shocks [Figs. 4(a) and (b)] are capable of energizing more particles to higher energies than quasi-perpendicular shocks [Fig. 4(c)]. $E = 10\ E_{sh}$ is marked by the vertical lines in Fig. 4. In Fig. 4(c), the ions are accelerated to higher energies faster by the quasi-perpendicular shock but achieve a nearly stable spectrum with a steep energy cut-off at $\sim 10\ E_{sh}$. In contrast, as shown in Figs. 4(a) and (b), the energy spectra produced by quasi-parallel shocks continue to grow further to higher energies. Only quasi-parallel shocks can accelerate a non-negligible population of ions to $\gtrsim 10\ E_{sh}$[15,16], meaning that any significant population of particles measured above this range in the experiment can only be produced by the quasi-parallel shock. We then define an ion acceleration efficiency as $\eta_i = N_{E>10\ E_{sh}}/N_{DS}$, where $N_{E>10E_{sh}}$ is the number of ions whose energy is above 10 E_{sh}, and N_{DS} is the number of ions in the downstream. For $\theta_n = 0°$, 30°, and 60° shocks, the efficiencies of $\eta_i \approx 0.14\%$, 0.06%, and 0.0004%, respectively, are obtained from the distributions at $t = 40\omega_{ci1}^{-1}$. Therefore, the parallel shocks are expected to be more efficient in particle acceleration. While ions can be accelerated to higher energies by quasi-parallel shocks, the experimentally relevant timescales explored here are still too short to obtain a power-law spectrum[3] that is usually seen in astrophysical observations of energized particles. Figures 4(d)−(f) indicate significant electron energization by the shocks, which will be discussed in Section IV(B).

Nevertheless, the simulations show that this experimental

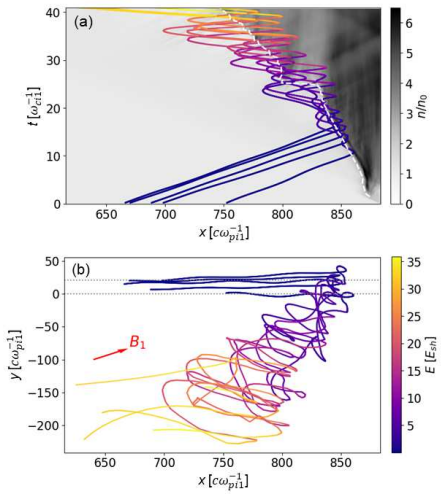

FIG. 3. Trajectories of some tracked ions in (a) x-t and (b) x-y plots. The color indicates their kinetic energies in the laboratory frame. In (a), the y-averaged density profile is shown in the background in grayscale, and the shock front is marked by the white dashed line. In (b), the periodic boundary conditions in the y-direction are post-processed to show a continuous 2-D space; the original y boundaries are marked by the dotted lines.

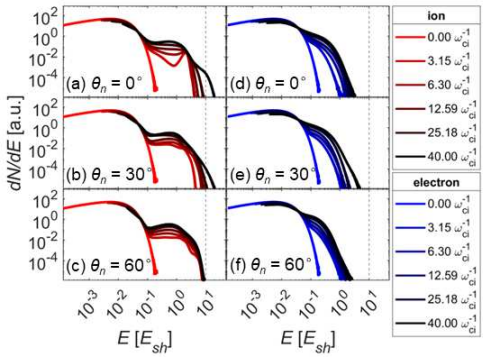

FIG. 4. Ion energy spectra of quasi-parallel (a) $\theta_n = 0°$, (b) $\theta_n = 30°$, and quasi-perpendicular (c) $\theta_n = 60°$ shocks. The electron energy spectra are shown in (d)-(f). Energies are in the laboratory frame.

achievable early-stage quasi-parallel shock has already: 1) formed a density compression $r \sim 4$ that Rankine-Hugoniot conditions[43] predict for a strong shock [Fig. 2]; 2) created an environment that allows ions to repetitively cross the shock front and gain energy [Fig. 3]; 3) energized a number of ions that exceed 10 E_{sh} [Fig. 4].

IV. UPSTREAM AND DOWNSTREAM PHYSICS

A. Wave excitation in the upstream

In quasi-parallel shocks, high-energy ions that are accelerated by the first-order Fermi process gyrate along the B field in the upstream. They also interact with ambient plasma and excite waves[5,46] as they escape upstream and travel in the ambient plasma. Figure 5(a) shows the B_z field profile at $t = 12.59\omega_{ci1}^{-1}$ in the $\theta_n = 0°$ simulations. Unlike downstream turbulence, apparent wave patterns are seen in the far upstream region (weakly perturbed, $x < 790c\omega_{pi1}^{-1}$). In Fig. 5(b), the Fourier spectrum of the upstream B_z field shows an X-shaped mode, whose arms are at an oblique angle of 65° to the k_x axis. In the weakly perturbed upstream region, we can use the upstream initial parameters in Table I to estimate the magnetohydrodynamic (MHD) wave velocities, $v_{ms1} \approx 2.17 v_{A1}$, where $v_{ms1} = \sqrt{v_{A1}^2 + c_{s1}^2}$ is the upstream magnetosonic wave velocity, $v_{A1} = B_1/\sqrt{4\pi m_i n_{i1}}$ is the upstream Alfvén velocity, $c_{s1} = \sqrt{\gamma k_B (T_{e1} + T_{i1})/m_i}$ is the upstream sound velocity, $\gamma = 5/3$ is the polytropic index, and k_B is Boltzmann constant. As the upstream magnetosonic waves and Alfvén waves propagate at their own characteristic velocities, the wavefront of the combined wave would show a propagation at an oblique angle of $arctan(v_{ms1}/v_{A1}) \approx 65°$, which agrees with the X-shaped mode in Fig. 5(b). Similarly, in Fig. 5(c), the Fourier spectrum of the upstream waves in the $\theta_n = 30°$ simulation also shows an X-shaped mode but with a tilt angle of 30°. Therefore, the far upstream waves are composed of two MHD waves, magnetosonic waves perpendicular to the B field, and Alfvén waves parallel to the B field. These MHD waves are excited by the accelerated energetic ions that travel through the upstream ambient plasma and deposit their energies. The ions are diffused in the upstream, slowed down, and caught up by the shock, then enter the downstream. Since the magnetic fields dominate the excited waves in the upstream, the ions are likely reflected by the magnetic fields. But this needs further study. The downstream turbulence acts as another diffusive mechanism that reflects the ions back to the upstream. This process repetitively reflects and accelerates the ions until they gain enough energy and finally escape[3,5]. Observing these waves in the simulation shows that the formation of the upstream, a critical stage in the formation of a quasi-parallel shock, is expected to be achievable in the NIF experiment.

B. Ion-electron energy partition in the downstream

In the downstream, energy partition between ions and electrons is also of interest. The Rankine-Hugoniot jump conditions describe the relationship between the states in the upstream and downstream of a steady-state shock[8,43]. Downstream temperature is predicted to be[8]

$$T_{i2} + T_{e2} = \frac{1}{5} m_i V_{sh}^2 \left(\frac{5\beta_1}{2M_{A1}^2} + 1 + \frac{2}{2M_{A1}^2} - \frac{1}{r^2} - \frac{2r}{M_{A1}^2} \right) \approx 3700\,\text{eV} \quad (1)$$

for a strong shock ($r \approx 4$). How this energy is partitioned between the ions and electrons is a question that can only be addressed by kinetic simulations. Figure 6 shows the history of the downstream ion and electron energy spectra in the $\theta_n = 30°$ simulations. An isotropization process between the two species is observed in the downstream region, which

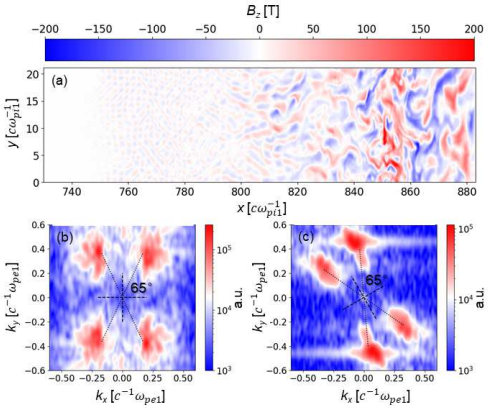

FIG. 5. (a) B_z field profile at $t = 12.59\omega_{ci1}^{-1}$ in the $\theta_n = 0°$ simulation. Fourier spectra of the far upstream B_z fields in the (b) $\theta_n = 0°$ and (c) $\theta_n = 30°$ simulations.

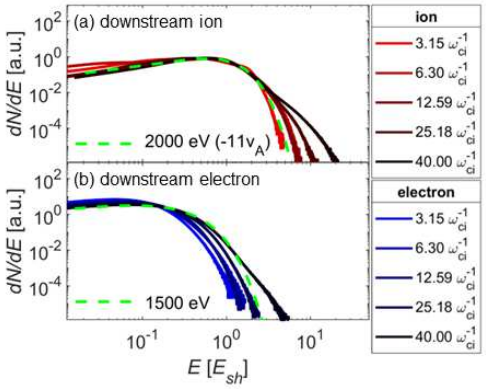

FIG. 6. Downstream (a) ion and (b) electron energy spectra in the $\theta_n = 30^\circ$ simulations. Energies are in the laboratory frame.

gives an energy partition of $T_{i2}/T_{e2} \approx 1.3$ within the simulation time. Reference Maxwellian energy distributions of $T = 1500$ eV and 2000 eV are also labeled in the figure. Note that the distributions and spectra in Fig. 6 are given in the laboratory frame, in which the upstream is stationary while the downstream moves at an Alfvénic Mach number higher than the piston. The bulk parts of the energy spectra show good agreement with the Maxwellian distributions, but both species have high-energy tails that extend out of the main distribution profiles at later times in Fig. 6, indicating particle acceleration.

The energy partition result implies a significant electron heating due to ion-electron energy exchange, which also agrees with planetary and astrophysical observations[47] that indicate $T_i/T_e \approx 0.5 - 30$ under different interstellar conditions. As a comparison, adiabatic electron heating, which is assumed in hybrid simulations, would give a downstream electron temperature $T_{e2} = T_{e1} \cdot r^{\gamma-1} \approx 250$ eV. Independent thermalization of each species would predict a temperature increase $\Delta T_i/\Delta T_e \approx m_i/m_e = 1836$, i.e., $\Delta T_e \approx 2$ eV. Both estimates are much smaller than the simulation result.

We note that this conclusion may only be valid for the low Mach number, quasi-parallel regime, in contrast to astrophysical observations where the Alfvénic Mach number is of the order of 100[23]. The isotropization process is likely the result of a complicated mixture of micro-instabilities, until turbulence is sufficiently developed. The relevant instabilities will be discussed in future publications.

This paper focused on ion acceleration, which is expected to be a key signature of the planned NIF experiments. However, non-thermal electrons were also observed in Figs. 4 and 6, indicating electron acceleration. In addition, collisionless ion-electron energy transfer could also play a role. Possible mechanisms are not currently understood and will be a future research topic.

V. CONCLUSIONS

Quasi-parallel shock formation relevant to laser-driven experiments on the NIF has been studied with 2-D PIC simulations. It is found that an early stage of quasi-parallel shock formation can be achieved on the NIF, and that energetic ions accelerated by the Fermi process are observable. Even so, the limited experimental extent in time and distance means that a power law energy spectrum does not have time to develop. However, one of the key features of DSA, ion repetitive crossing of the shock front by scattering from waves and turbulence is seen in the simulations. We expect that the shock formation and structure are essentially captured by these 2-D simulations, based on observed similarity between our 1-D and 2-D simulations. This is further supported by the observed similarity between 2-D and 3-D hybrid simulations[16]. However, whether particle acceleration or ion-electron coupling may change in 3-D remains to be studied in the future.

More importantly, the simulations confirm that quasi-parallel shocks are capable of energizing more particles and creating energy spectra that extend further than from quasi-perpendicular shocks. Under experimental conditions, our simulations indicate that a population of ions with energies above $10E_{sh}$ can only be effectively produced by quasi-parallel shocks. Upstream waves excited by these accelerated ions are identified as parallel Alfvén waves and perpendicular magnetosonic waves. In the downstream, ions and electrons reached an energy partition $T_{i2}/T_{e2} \approx 1.3$. These findings, including density compression, high energy ions, turbulent structures produced by the shock, and the temperatures of ions and electrons, provide experimental observables that will be tested in the experiments on the NIF. Most importantly, energetic particles accelerated by quasi-parallel shocks have never been experimentally observed before. This NIF platform aims to validate the experimental capability of quasi-parallel shock studies.

ACKNOWLEDGMENTS

The authors would like to thank Dr. Damiano Caprioli for the useful discussions. This material is based upon work supported by the Department of Energy [National Nuclear Security Administration] University of Rochester "National Inertial Confinement Fusion Program" under Award No. DE-NA0004144, the Department of Energy under Award Nos. DE-SC0020431 and DE-SC0024566, and the resources of the National Energy Research Scientific Computing Center (NERSC), a U.S. Department of Energy Office of Science User Facility located at Lawrence Berkeley National Laboratory. The authors thank the UCLA-IST OSIRIS consortium for the use of OSIRIS.

This report was prepared as an account of work sponsored by an agency of the U.S. Government. Neither the U.S. Government nor any agency thereof, nor any of their employees, makes any warranty, express or implied, or assumes any legal liability or responsibility for the accuracy, completeness, or usefulness of any information, apparatus, product, or pro-

cess disclosed, or represents that its use would not infringe privately owned rights. Reference herein to any specific commercial product, process, or service by trade name, trademark, manufacturer, or otherwise does not necessarily constitute or imply its endorsement, recommendation, or favoring by the U.S. Government or any agency thereof. The views and opinions of authors expressed herein do not necessarily state or reflect those of the U.S. Government or any agency thereof.

DATA AVAILABILITY STATEMENT

The data that support the findings of this study are available from the corresponding author upon reasonable request.

[1]E. Fermi, "On the origin of the cosmic radiation," Physical review **75**, 1169 (1949).
[2]W. Axford, E. Leer, and G. Skadron, "The acceleration of cosmic rays by shock waves," in *International cosmic ray conference*, Vol. 11 (Springer, 1977).
[3]A. Bell, "The acceleration of cosmic rays in shock fronts–i," Monthly Notices of the Royal Astronomical Society **182**, 147–156 (1978).
[4]A. Bell, "The acceleration of cosmic rays in shock fronts–ii," Monthly Notices of the Royal Astronomical Society **182**, 443–455 (1978).
[5]R. D. Blandford and J. P. Ostriker, "Particle acceleration by astrophysical shocks," Astrophysical Journal, Part 2-Letters to the Editor, vol. 221, Apr. 1, 1978, p. L29-L32. **221**, L29–L32 (1978).
[6]M. S. Longair, *High energy astrophysics* (Cambridge university press, 2010).
[7]G. Morlino, "The role of ionization in the shock acceleration theory," Monthly Notices of the Royal Astronomical Society **412**, 2333–2344 (2011).
[8]Y. Zhang, J. R. Davies, P. V. Heuer, and C. Ren, "Kinetic simulation study of magnetized collisionless shock formation on a terawatt laser system," Physics of Plasmas **28** (2021).
[9]Y. Zhang, J. R. Davies, P. V. Heuer, and C. Ren, "Erratum: "Kinetic simulation study of magnetized collisionless shock formation on a terawatt laser system" [Phys. Plasmas 28, 072111 (2021)]," Physics of Plasmas **28** (2021).
[10]P. Heuer, M. Weidl, R. Dorst, D. Schaeffer, S. Tripathi, S. Vincena, C. Constantin, C. Niemann, and D. Winske, "Laser-produced plasmas as drivers of laboratory collisionless quasi-parallel shocks," Physics of Plasmas **27** (2020).
[11]D. Schaeffer, W. Fox, J. Matteucci, K. Lezhnin, A. Bhattacharjee, and K. Germaschewski, "Kinetic simulations of piston-driven collisionless shock formation in magnetized laboratory plasmas," Physics of Plasmas **27** (2020).
[12]C. Niemann, W. Gekelman, C. Constantin, E. Everson, D. Schaeffer, A. Bondarenko, S. Clark, D. Winske, S. Vincena, B. Van Compernolle, *et al.*, "Observation of collisionless shocks in a large current-free laboratory plasma," Geophysical Research Letters **41**, 7413–7418 (2014).
[13]D. Schaeffer, W. Fox, D. Haberberger, G. Fiksel, A. Bhattacharjee, D. Barnak, S. Hu, and K. Germaschewski, "Generation and evolution of high-mach-number laser-driven magnetized collisionless shocks in the laboratory," Physical review letters **119**, 025001 (2017).
[14]D. B. Schaeffer, W. Fox, R. Follett, G. Fiksel, C. Li, J. Matteucci, A. Bhattacharjee, and K. Germaschewski, "Direct observations of particle dynamics in magnetized collisionless shock precursors in laser-produced plasmas," Physical review letters **122**, 245001 (2019).
[15]W. Yao, A. Fazzini, S. Chen, K. Burdonov, P. Antici, J. Béard, S. Bolaños, A. Ciardi, R. Diab, E. Filippov, *et al.*, "Laboratory evidence for proton energization by collisionless shock surfing," Nature Physics **17**, 1177–1182 (2021).
[16]D. Caprioli and A. Spitkovsky, "Simulations of ion acceleration at non-relativistic shocks. i. acceleration efficiency," The Astrophysical Journal **783**, 91 (2014).
[17]R. P. Drake, "The design of laboratory experiments to produce collisionless shocks of cosmic relevance," Physics of Plasmas **7**, 4690–4698 (2000).
[18]E. M. Campbell and W. J. Hogan, "The national ignition facility-applications for inertial fusion energy and high-energy-density science," Plasma Physics and Controlled Fusion **41**, B39 (1999).
[19]G. H. Miller, E. I. Moses, and C. R. Wuest, "The national ignition facility: enabling fusion ignition for the 21st century," Nuclear fusion **44**, S228 (2004).
[20]E. Moses, R. Boyd, B. Remington, C. Keane, and R. Al-Ayat, "The national ignition facility: Ushering in a new age for high energy density science," Physics of Plasmas **16** (2009).
[21]K. Manes, D. Kalantar, P. Miller, J. Heebner, E. Bliss, D. Spec, T. Parham, P. Whitman, P. Wegner, *et al.*, "Description of the nif laser," Fusion Science and Technology **69**, 25–145 (2016).
[22]H. Abu-Shawareb, R. Acree, P. Adams, J. Adams, B. Addis, R. Aden, P. Adrian, B. Afeyan, M. Aggleton, L. Aghaian, *et al.*, "Achievement of target gain larger than unity in an inertial fusion experiment," Physical Review Letters **132**, 065102 (2024).
[23]F. Fiuza, G. Swadling, A. Grassi, H. Rinderknecht, D. Higginson, D. Ryutov, C. Bruulsema, R. Drake, S. Funk, S. Glenzer, *et al.*, "Electron acceleration in laboratory-produced turbulent collisionless shocks," Nature physics **16**, 916–920 (2020).
[24]P. V. Heuer, M. S. Weidl, R. S. Dorst, D. B. Schaeffer, S. K. Tripathi, S. Vincena, C. G. Constantin, C. Niemann, L. B. Wilson III, and D. Winske, "Laboratory observations of ultra-low-frequency analog waves driven by the right-hand resonant ion beam instability," The Astrophysical Journal Letters **891**, L11 (2020).
[25]P. Heuer, M. Weidl, R. Dorst, D. Schaeffer, A. Bondarenko, S. Tripathi, B. Van Compernolle, S. Vincena, C. Constantin, C. Niemann, *et al.*, "Observations of a field-aligned ion/ion-beam instability in a magnetized laboratory plasma," Physics of Plasmas **25** (2018).
[26]D. Caprioli and A. Spitkovsky, "Simulations of ion acceleration at non-relativistic shocks. ii. magnetic field amplification," The Astrophysical Journal **794**, 46 (2014).
[27]D. Caprioli and A. Spitkovsky, "Simulations of ion acceleration at non-relativistic shocks. iii. particle diffusion," The Astrophysical Journal **794**, 47 (2014).
[28]H.-b. Cai, X.-x. Yan, P.-l. Yao, and S.-p. Zhu, "Hybrid fluid–particle modeling of shock-driven hydrodynamic instabilities in a plasma," Matter and Radiation at Extremes **6** (2021).
[29]E. Zhang, H. Cai, W. Zhang, Q. Liu, H. Luo, G. Zhu, M. Luo, and S. Zhu, "Influence of the electron thermal conduction and ion kinetic effects on the structure of collisional plasma shocks," Physics of Plasmas **29** (2022).
[30]A. Le, A. Stanier, L. Yin, B. Wetherton, B. Keenan, and B. Albright, "Hybrid-vpic: An open-source kinetic/fluid hybrid particle-in-cell code," Physics of Plasmas **30** (2023).
[31]A. Bondarenko, D. Schaeffer, E. Everson, S. Clark, B. Lee, C. Constantin, S. Vincena, B. Van Compernolle, S. Tripathi, D. Winske, *et al.*, "Collisionless momentum transfer in space and astrophysical explosions," Nature Physics **13**, 573–577 (2017).
[32]R. A. Fonseca, L. O. Silva, F. S. Tsung, V. K. Decyk, W. Lu, C. Ren, W. B. Mori, S. Deng, S. Lee, T. Katsouleas, *et al.*, "Osiris: A three-dimensional, fully relativistic particle in cell code for modeling plasma based accelerators," in *Computational Science—ICCS 2002: International Conference Amsterdam, The Netherlands, April 21–24, 2002 Proceedings, Part III 2* (Springer, 2002) pp. 342–351.
[33]K. Quest, "Theory and simulation of collisionless parallel shocks," Journal of Geophysical Research: Space Physics **93**, 9649–9680 (1988).
[34]D. Burgess and M. Scholer, *Collisionless shocks in space plasmas: Structure and accelerated particles* (Cambridge University Press, 2015).
[35]A. Beresnyak, *2023 NRL plasma formulary* (Naval Research Laboratory Washington, DC, 2023).
[36]D. Maywar, J. Kelly, L. Waxer, S. Morse, I. Begishev, J. Bromage, C. Dorrer, J. Edwards, L. Folnsbee, M. Guardalben, *et al.*, "Omega ep high-energy petawatt laser: progress and prospects," in *Journal of Physics: Conference Series*, Vol. 112 (IOP Publishing, 2008) p. 032007.
[37]J. Kelly, L. Waxer, V. Bagnoud, I. Begishev, J. Bromage, B. Kruschwitz, T. Kessler, S. Loucks, D. Maywar, R. McCrory, *et al.*, "Omega ep: High-energy petawatt capability for the omega laser facility," in *Journal de Physique IV (Proceedings)*, Vol. 133 (EDP sciences, 2006) pp. 75–80.
[38]L. Waxer, D. Maywar, J. Kelly, T. Kessler, B. Kruschwitz, S. Loucks, R. McCrory, D. Meyerhofer, S. Morse, C. Stoeckl, *et al.*, "High-energy

petawatt capability for the omega laser," Optics and photonics news **16**, 30–36 (2005).
[39]S. P. Gary, *Theory of space plasma microinstabilities*, 7 (Cambridge university press, 1993).
[40]J. B. McBride, E. Ott, J. P. Boris, and J. H. Orens, "Theory and simulation of turbulent heating by the modified two-stream instability," The Physics of Fluids **15**, 2367–2383 (1972).
[41]R. Treumann, "Fundamentals of collisionless shocks for astrophysical application, 1. non-relativistic shocks," The Astronomy and Astrophysics Review **17**, 409–535 (2009).
[42]P. Pongkitiwanichakul, D. Schaeffer, W. Fox, D. Ruffolo, J. Donaghy, and K. Germaschewski, "Kinetic simulations comparing quasi-parallel and quasi-perpendicular piston-driven collisionless shock dynamics in magnetized laboratory plasmas," Physics of Plasmas **31** (2024).
[43]D. A. Tidman, N. A. Krall, and M. Dryer, "Shock waves in collisionless plasmas," American Journal of Physics **40**, 1055–1055 (1972).
[44]D. A. Gurnett and A. Bhattacharjee, *Introduction to plasma physics: With space, laboratory and astrophysical applications* (Cambridge University Press, 2017).
[45]L. O. Drury, "An introduction to the theory of diffusive shock acceleration of energetic particles in tenuous plasmas," Reports on Progress in Physics **46**, 973 (1983).
[46]M. Scholer and D. Burgess, "The role of upstream waves in supercritical quasi-parallel shock re-formation," Journal of Geophysical Research: Space Physics **97**, 8319–8326 (1992).
[47]P. Ghavamian, S. J. Schwartz, J. Mitchell, A. Masters, and J. M. Laming, "Electron-ion temperature equilibration in collisionless shocks: the supernova remnant-solar wind connection," Space Science Reviews **178**, 633–663 (2013).